ACS APPLIED MATERIALS & INTERFACES

Research Article

www.acsami.org

Fabrication of Polystyrene/ZnO Micronano Hierarchical Structure Applied for Light Extraction of Light-Emitting Devices

Peng Mao,[†,‡] Amulya krishna Mahapatra,[†] Jing Chen,[§] Minrui Chen,[†] Guanghou Wang,[†,‡] and Min Han*[,†,‡]

[†]National Laboratory of Solid State Microstructures and Department of Materials Science and Engineering, Nanjing University, Nanjing 210093, China

[‡]Collaborative Innovation Center of Advanced Microstructures, Nanjing University, Nanjing 210093, China

[§]College of Electronic Science and Engineering, Nanjing University of Posts and Telecommunications, Nanjing 210046, China

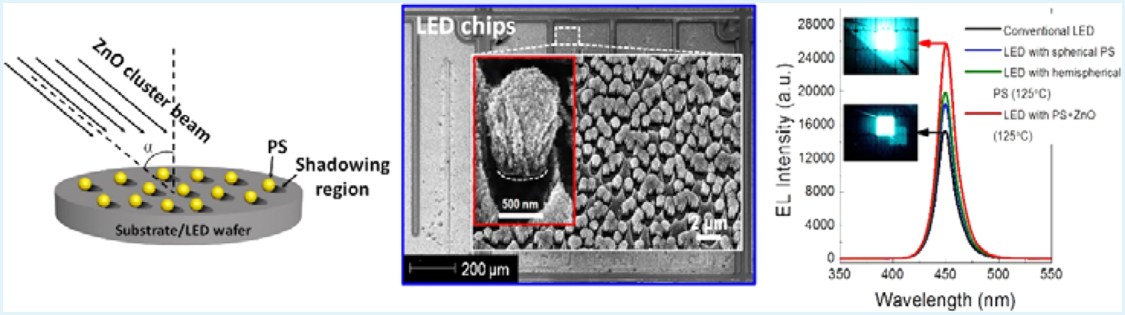

ABSTRACT: Polystyrene(PS)/ZnO micronano hierarchical structures were fabricated on a flat surface by depositing ZnO nanoparticles from a cluster beam at oblique incidence on the surface predeposited with PS microspheres. The hierarchical structure was composed of submicron-sized PS particle layers covered with dense films of columnar ZnO nanoparticle piles separated with nanoscale pores. It was demonstrated that the cooperative effect that combines the microlens function of the PS microspheres and the enhanced Rayleigh scattering of the ZnO nanoparticle porous layers can be used to greatly reduce the total internal reflection at the medium−air interface. The PS/ZnO hierarchical structures were fabricated on the surface of GaN-based light-emitting diode (LED) chips to enhance the light-extraction efficiency. A 77.7% improvement on the light-output power was realized, which was much greater than that obtained with the PS microstructures alone.

KEYWORDS: *light extraction, hierarchical structures, ZnO nanoparticles, cluster beam, light-emitting device*

1. INTRODUCTION

Light-emitting diodes (LEDs) have been studied intensively for their potential use in display and lighting products. They have promising advantages of high efficiency, long lifetime, and low power consumption.[1,2] GaN-based LED is one of the most commonly used LEDs. However, GaN-based LEDs display a low light-output power (LOP) compared to the theoretical value.[3] LOP could be improved through enhancement in internal quantum efficiency (IQE) and light-extraction efficiency (LEE). IQE has been achieved more than 80% through the improvement on the device fabrication techniques.[4,5] However, LEE is still low, mainly due to the considerable loss of generated light in total internal reflection (TIR) caused by the large difference in refractive index of GaN (n = 2.43) and air (n = 1).[6] It should be noted that only 4% of the generated light can escape out of the LEDs.[7] Most of the light from the quantum wells is internally reflected at the LED and air interface, trapped inside the device, and ultimately converted to heat, resulting in a significant reduction in the light-extraction efficiency.

To enhance the LOP of GaN-based LEDs, a variety of structures with microscale and/or nanoscale features have been incorporated into LEDs. Such features include photonic crystals,[8−11] conductive omnidirectional reflectors,[12,13] microlens arrays,[14−16] plasmonic nanostructure,[17−19] nanorods,[6,20,21] and surface roughening of current spreading layer.[22,23] They have been demonstrated to enhance the device performance largely by overcoming TIRs. Most studies have been focused on surface texturing of micrometer size due to the ease of fabrication, among which transparent electrode texturing and patterning is one of the commonly used effective methods. For example, the LOP of the LEDs with periodic microcircle structures on the indium tin oxide (ITO) layer exhibited a 46.4% enhancement compared to the conventional LEDs.[24] The use of microlens arrays on GaN-based LEDs has been demonstrated as one of the most effective techniques in improving LEE.[7,14,15,25] The significant increase in the output

Received: June 4, 2015
Accepted: August 17, 2015
Published: August 17, 2015

DOI: 10.1021/acsami.5b04911
ACS Appl. Mater. Interfaces 2015, 7, 19179−19188

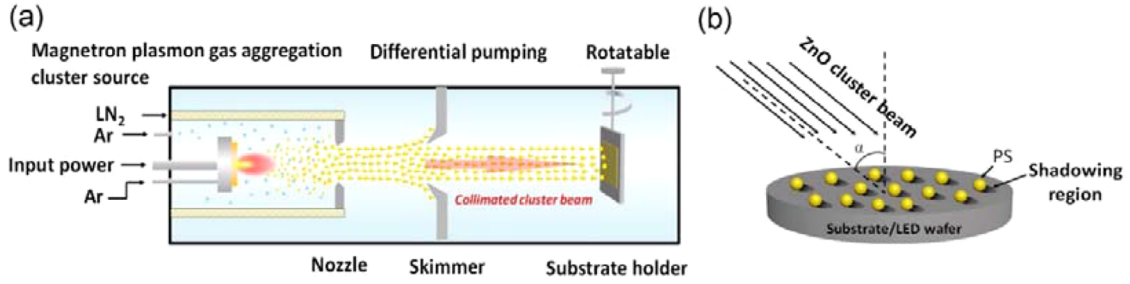

Figure 1. (a) Schematic diagram of a magnetron plasma gas aggregation cluster beam deposition process. (b) Sketch illustrating the oblique-angle cluster beam deposition process; α is the cluster beam incident angle measured from the substrate normal.

power of the LEDs with microlens arrays presumably can be attributed to the increase in its effective photon escape cone and reduce Fresnel reflection in the ITO/air interface.[14] However, most of the ITO texturing and patterning methods involve high temperature and a dry etching process, which could cause some sacrifice of the favorable electrical properties of the LEDs. For next-generation applications of high-efficiency LEDs, further improvement of the LEE is required.

Currently, microscale/nanoscale hierarchical structures have been studied for improving the LOP of LEDs. It was shown that introduction of hierarchical structures was also a promising way to suppress the total internal light loss because they could make a dual enhancement of the LEE, which was achieved by combining two different effects following microscale or nanoscale mechanisms toward TIR reduction. For example, Sheu et al.[26] showed that the wall-plug efficiency of LEDs with textured ITO/GZO (Ga-doped ZnO) composite could be markedly improved by 45% as compared to conventional LEDs. Lee et al.[27] also showed that the luminous intensity of AlGaInP-based metal-bonding LEDs with micro- (microbowl arrays) and nanoscale (nanorods) textured surface could be enhanced 65.8% under 20 mA current injection as compared with the plane surface LEDs. LEDs with hierarchical surfaces consisting of p-GaN microdomes and SiO_2 nanorods exhibited a light-output improvement of 36.8%.[28] Recently, Kim et al.[29] demonstrated that a hybrid structure comprising ZnO nanorod arrays grown on the NiCoO hemispherical lens showed an increase of light extraction by 3.8 and 6.2 times compared to LEDs with bare NiCoO nanoparticles and without any nanoparticles, respectively. The enhancement was attributed to the enlarged escape angle cone and increased probability of light scattering. We have shown that a thick stacking of dense TiO_2 nanoparticles with nanoscale porosity could be used to significantly enhance the LEE of LED,[30] and the mechanism should be attributed to Rayleigh scattering induced by refractive index fluctuations among the nanoparticle layer,[30,31] rather than the reduction of Fresnel reflection.

Oblique-angle deposition has been proven to be an effective method to fabricate porous nanostructures, and it was recently applied for improving LOP of LEDs. Lin and Lee showed that the light-output power of the LED covered with ITO nanorod arrays fabricated by oblique-angle deposition technique could be enhanced 26.4% as compared with the conventional LED and could be attributed to the nanorod surface morphology and the matching of refractive index obtained by the ITO nanorod arrays.[32] By performing oblique-angle cluster beam deposition, we fabricated columnar TiO_2 nanoparticle piles separated with nanoscale pores on the surfaces of GaN LEDs to enhance their light output.[30]

Despite many studies being conducted on the improving LOP of LEDs with microscale and/or nanoscale structures, to date most of the approaches have been focused on the reduction of the Fresnel reflection in the dielectric/air interface. Especially, the light-extraction effects of nanostructures, such as the waveguiding effect, the multiple tilted surfaces, and the graded refractive indices, were considered independently. Although hierarchical structures were fabricated, they were not optimized to apply the cooperative effect between the microscale structures and the nanoscale structure. In the present work, we employ oblique-angle cluster beam deposition to fabricate microscale/nanoscale hierarchical structures combining polystyrene (PS) microsphere arrays and ZnO nanoparticle porous layers on the surface of GaN-based LEDs to reduce TIR loss and enhance the LEE. We perform a quantitative measurement on the incident angle-dependent TIR extraction efficiency of the hierarchical structures. We report an extra enhancement on the LEE, which is attributed to the cooperative effect of the PS hemisphere arrays that act as microlens and the ZnO nanoparticle porous layers that generate enhanced Rayleigh scattering.

2. EXPERIMENTAL SECTION

2.1. Fabrication of GaN-Based LED Chips. GaN-based LED chips were fabricated by sequentially growing undoped GaN (u-GaN, 2 μm), n-GaN (2 μm), five periods of InGaN/GaN multiple quantum wells (MQWs), p-GaN (250 nm), indium tin oxide (200 nm), and p- and n-type Cr/Au electrodes on c-plane sapphire substrates (400 μm), using a metal−organic chemical vapor deposition (MOCVD) process. The details of the LED-fabrication process can be found elsewhere.[30,33] The fabricated LED chips (set A) and silica glasses (set B) were used as substrates in equal experimental condition for further treatment.

2.2. Deposition Submonolayer PS Microsphere. The monodispersed PS microspheres (mean size 0.5 μm, size distribution $\lesssim$3% CV, solid 10% w/w) used in the work was purchased from Duke Scientific Corps. The monolayer of PS microspheres was formed on LEDs by using the spin-coating process. The PS microspheres were diluted 20 times, spin-coated on the substrates at a rotation speed of 250 rpm for 120 s and 800 rpm for 200 s, and finally dried in air naturally.

2.3. Fabrication of PS/ZnO Hierarchical Structure. An oblique-angle cluster beam deposition process[30] was used to deposit ZnO nanoparticle layers on the LED surface with PS microspheres. In such a process, the PS microspheres randomly distributed on the substrate produced shadow regions that the incident nanoparticle flux could not reach, while on the nonshadow regions (tops of the PS microspheres) the incident cluster flux deposited preferentially. As a result, the nanoparticles piled up and formed a PS/ZnO based hierarchical structure.

In our fabrication, ZnO nanoparticles were generated in a magnetron plasma gas aggregation cluster source[34−36] and deposited on substrates obliquely, as shown in Figure 1a. The deposition was

DOI: 10.1021/acsami.5b04911
ACS Appl. Mater. Interfaces 2015, 7, 19179−19188

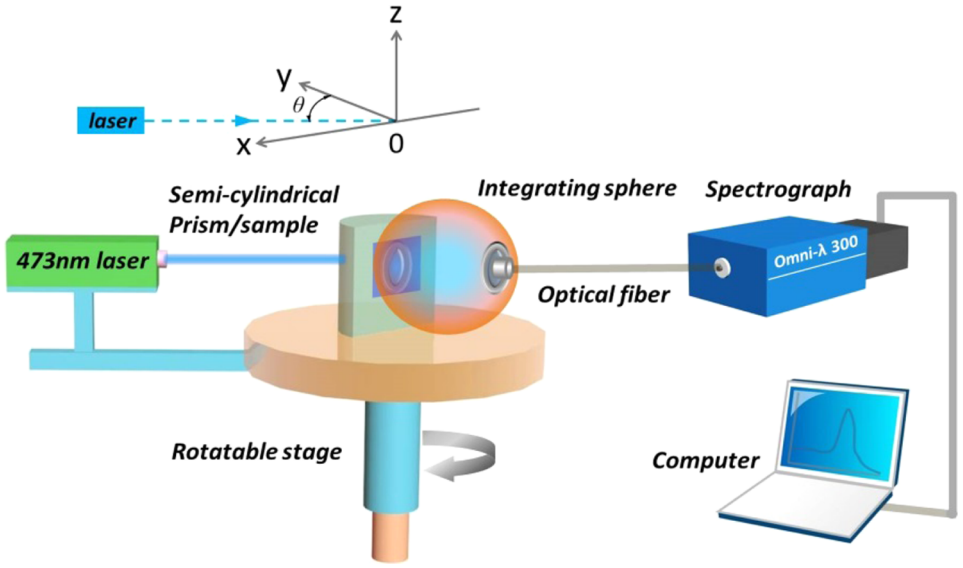

Figure 2. Schematic diagram of the angle-resolved light-transmission measurement system.

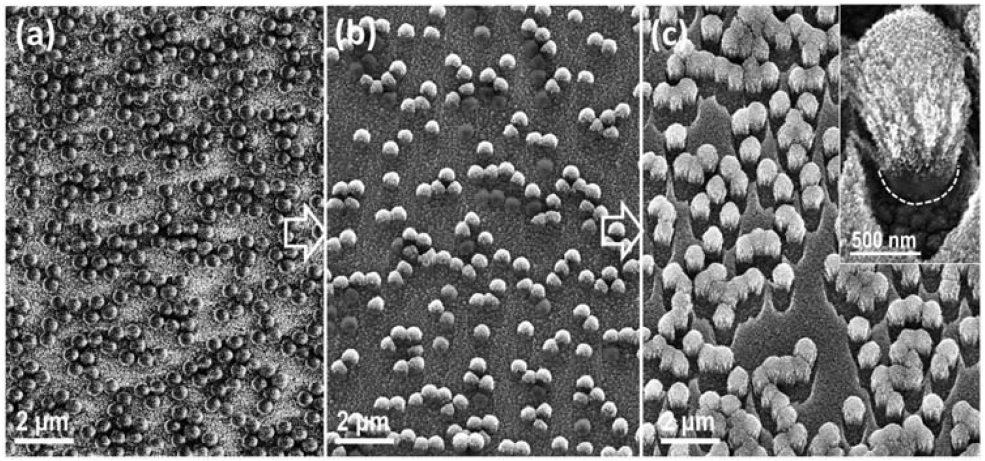

Figure 3. SEM micrographs of the porous PS/ZnO hierarchical structure at different nanoparticle deposition stages, which show the evolution of structure in the deposition process. (a) Before the deposition, the PS microspheres are randomly distributed on the LED chip surface. (b) In the deposition process, the 500 nm sized PS microspheres acted as obstacles that accumulated deposited nanoparticles on the faces exposing to the beam. (c) After the deposition, the formations of column-like structures on PS microspheres are evident. The inset shows a high-magnification SEM image of an individual PS microsphere covered with ZnO nanoparticles.

performed in a high-vacuum chamber equipped with the cluster source. A ZnO target with high purity (99.999%) was used as the sputtering target. An intermediate frequency pulse power supply was used for the sputtering of ZnO target in argon gas (purity, 99.999%) ambient with a pressure of ∼100 Pa, maintained by passing argon gas to the liquid nitrogen-cooled aggregation tube. A stable magnetron discharge ran with input power, frequency, and duty ratio of 130 W, 40 kHz, and 55%, respectively. Sputtered ZnO molecules lost energy by colliding with the cooled argon gas in the aggregation tube and formed nanoparticles. The nanoparticles were swept by the gas stream into high vacuum through a nozzle, forming a collimated nanoparticle beam with a high speed of ∼1000 m/s.[35] Thus, the nanoparticles deposited and stuck on the substrate or LED chip surface firmly. The substrate was tilted so that the incident nanoparticle beam direction made a 65° angle against the substrate surface normal, as shown in Figure 1b. The deposition was carried out at a rate of 1.5 ± 0.1 Å/s for 45 min. In situ annealing was carried out for 10 min at 125 °C, after the deposition. Under annealing, the PS spheres deformed into hemispheres. In the end, three kinds of samples were prepared on both set A and set B substrates: (i) spin-coated PS microspheres, (ii) annealed PS microspheres (PS hemispheres), and (iii) annealed PS/ZnO hierarchical structure.

A field-emission scanning electron microscope (FE-SEM, ZEISS SIGMA) was used to study the surface morphology of the samples. Light-output measurement and the electrical characteristics of the GaN-based LEDs were measured using an on-wafer testing configuration (IPT 6000 LED chip/wafer probing system). The system was composed of an optical parameter analyzer with an integrating half-sphere mounted above the LEDs. Far-field radiation patterns of LEDs were measured by an LED goniophotometer (LED626, EVERFINE Corporation).

2.4. Incident Angle-Resolved Light-Transmission Measurements. The light-transmission properties of the PS/ZnO hierarchical structure were inspected on a homemade spectrophotometer containing a hemicylindrical prism sample stage. The samples were directly adhered to the flat face of the hemicylindrical silica glass prism. The gap between the sample substrate and the prism was filled with refractive index matching liquid of refractive index n = 1.46, so light could transmit from the prism into the sample with little loss.[37] An integrating sphere was placed behind the prism to collect the transmitted light. We could then directly measure the light

DOI: 10.1021/acsami.5b04911
ACS Appl. Mater. Interfaces 2015, 7, 19179−19188

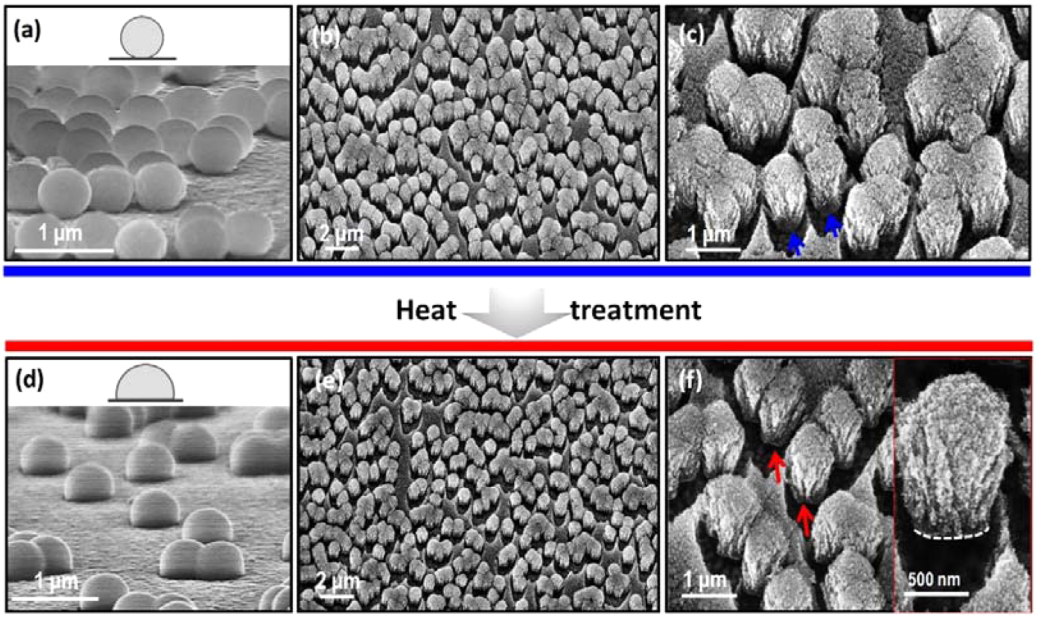

Figure 4. (a) SEM image of spherical PS particles. (b) SEM image of PS/ZnO hierarchical structure. (c) High-magnification SEM image of PS/ZnO hierarchical structure. The blue arrow indicates the exposed half face of the PS microsphere. (d) SEM image of hemispherical PS particles after heat treatment. (e) SEM image of PS/ZnO hierarchical structure after heat treatment at 125 °C. (f) High-magnification SEM image of PS/ZnO hierarchical structure after heat treatment. The red arrow indicates that the exposed half faces of the PS microsphere were almost invisible after heat treatment. The inset shows an SEM image of a single ZnO nanoparticle-covered PS microsphere after heat treatment.

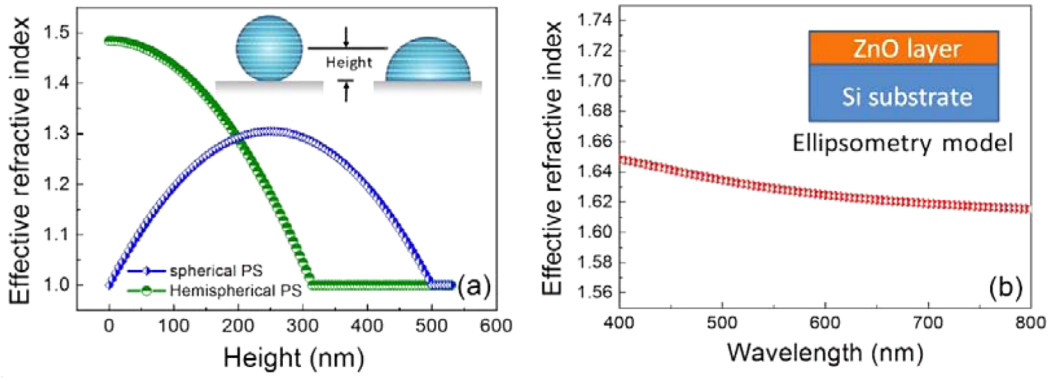

Figure 5. (a) Calculated values of effective refractive index of a spherical and a hemispherical PS microparticle array. The values of refractive index of air, PS, and silica glass substrate are 1, 1.59, and 1.5, respectively. (b) Measured optical refractive index of porous ZnO nanoparticle layer obliquely deposited on substrate with an incident angle of 65°.

transmission from the sample to air as a function of the incident angle θ. The critical angle of silica glass is θ_c = 43.0°, determined by the refractive index of 1.46. A 473 nm laser beam passed through the circular edge of the prism and impinged on the center of the flat face of the hemicylindrical prism where the samples were attached. The incident angle θ of the laser beam could be varied with an angular resolution of 2°. Far-field transmission spectra were collected from the flat surface of the prism. The light was collected by the integrating sphere and propagated to the spectrometer (Zolix Omni-λ 300) via an optical fiber. Both the prism and the integrating sphere were installed at the center of a scanning stage so that the incident angles of the illumination light could be varied. A schematic diagram of the angle-resolved light-transmission measurement system is shown in Figure 2.

3. RESULTS AND DISCUSSION

3.1. Characterization of the PS/ZnO Hierarchical Structure. Typical SEM micrographs of the PS/ZnO hierarchical structure at different deposition stages are shown in Figure 3. As shown in Figure 3a, the PS microspheres are randomly distributed on the LED chip surface. When the nanoparticles were deposited on the surface obliquely from the cluster beam, the 500 nm sized PS microspheres acted as obstacles that accumulated deposited nanoparticles (7 nm diameter on average) on the faces exposed to the beam (as shown in Figure 3b) and prevented nanoparticles from being deposited in the shadow regions. As shown in Figure 3c, the formations of column-like structures on PS microspheres are evident. Therefore, the oblique deposition generates two important contributions to the morphology formation: (a) due to the shadowing and self-shadowing effects, ZnO nanoparticles could not deposit on the shadow region of the PS microspheres and the deposited ZnO nanoparticles, which induced porous structures; (b) with heavy deposition mass, ZnO nanoparticles preferentially piled up, which formed columnar nanostructures. From the high-magnification SEM image presented as an insert in Figure 3c, which shows an individual PS microsphere covered with ZnO nanoparticles,

DOI: 10.1021/acsami.5b04911
ACS Appl. Mater. Interfaces 2015, 7, 19179−19188

one can see that the hierarchical structure consists of two components: the unexposed half face of the PS microsphere that is free of ZnO nanoparticle coverage and the columnar ZnO nanoparticle piles at the top of the PS microsphere that is exposed to the nanoparticle beam. In Figure 3c, the clean LED wafer surface without ZnO nanoparticle coverage can easily be distinguished (the dark areas adjacent to the PS microspheres).

Parts a–f of Figure 4 compare the morphologies of the PS/ZnO hierarchical structures before and after 125 °C annealing. After heat treatment, the spherical PS particles changed to be hemispheres and welded onto the substrate surface, as shown in Figure 4a and e. The formation of the PS hemispheres greatly enhanced the mechanical stability of the hierarchical structures since they adhered strongly to the substrate with large contact areas.[38] Furthermore, the ZnO nanoparticles deposited with relatively high kinetic energies and were subjected to some sintering in the postannealing process, which generated rigid columnar aggregations of ZnO nanoparticles. The deformation of the PS microspheres also induced deformation of the PS/ZnO hierarchical structure. After heat treatment, the PS microspheres were almost invisible, as can be seen in Figure 4f. This deformation is propitious to the light extraction of LEDs, which will be discussed later.

3.2. Effective Refractive Index Characterization. Refractive index is an important parameter on the analysis of the light-extraction mechanism of fabricated hierarchical structures. For a submonolayer of microparticles, effective refractive index changes with the height along the layer thickness. The effective refractive index (n_{eff}) is a spatial average of the refractive index of air and the discontinuous medium. Figure 5a shows the calculated values of effective refractive index of a spherical and a hemispherical PS microparticle array. They were calculated on the basis of the structure depicted in the inset in Figure 5a as[38]

$$n_{eff} = \frac{n_{air}A_{air} + n_{PS}A_{PS}}{A_{air} + A_{PS}} \quad (1)$$

where n_{air} and n_{PS} (~1.59 in the visible spectrum) are the refractive indices of air and PS and A_{air} and A_{PS} are the area fractions of air and PS colloidal particles at a certain height, respectively. As shown, along the layer thickness, the effective refractive index of the spherical PS microparticle layer first gradually increases and then decreases with the increase in height. For the hemispherical PS microparticle layer, the effective refractive index shows a monotonous decrease with the increase of height. This indicates that the hemispherical PS microparticle arrays have a graded refractive index that gradually changes from the air to the substrate surface, similar to that of moth-eye nanostructures for Fresnel reflection reduction.[39] Figure 5b plots the effective refractive index of a porous ZnO nanoparticle film obliquely deposited on a substrate with an incident angle of 65° as a function of wavelength. The data were measured with an ellipsometer. At the wavelength of 450 nm, the measured refractive index of the ZnO nanoparticle layer is 1.64, whereas the refractive index of bulk ZnO is ~2.11, which indicates that the fabricated ZnO nanoparticle film has a porous structure composed of air and aggregated ZnO nanoparticles. We have demonstrated previously that such nanoparticle aggregations in the nanoporous structures could display an enhanced Rayleigh scattering due to the strong contrast in the refractive index between pores and nanoparticles.[30] The PS/ZnO hybrid structure can be considered as a medium containing PS hemispheres immersed in the ZnO nanoparticle porous layer. Therefore, its effective refractive index can be calculated as

$$n_{eff} = \frac{n_{p\text{-}ZnO}A_{p\text{-}ZnO} + n_{PS}A_{PS}}{A_{p\text{-}ZnO} + A_{PS}} \quad (2)$$

where $n_{p\text{-}ZnO}$ is the refractive index of ZnO nanoparticle porous layer. At 450 nm wavelength, the average effective refractive index of the hybrid PS/ZnO layer is calculated to be ~1.62, which matches well between the refractive index of air and the ITO layer on LED chip.

3.3. Light-Transmission Properties of the PS/ZnO Hierarchical Structure. To visualize the transmission characteristics of the PS/ZnO hierarchical structures, a white screen was placed behind the flat surface of the silica glass prism to display the spots of the transmitted light. Figure 6a exhibits

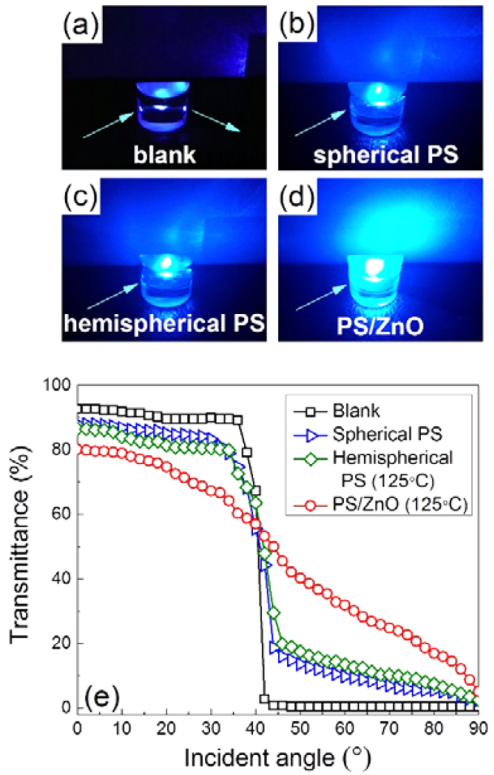

Figure 6. Images of the spots of transmitted light extracted from the (a) blank silica glass hemicylindrical prism, (b) glass prism with spherical PS microparticle layer, (c) glass prism with hemispherical PS microparticle layer, and (d) glass prism with PS/ZnO hierarchical structure. (e) Experimental light transmittance curves of the extracted light vs incident angle of the laser for the above four samples.

the images of the spots formed with the transmitted light from the blank silica glass substrate, glass with PS microspheres, glass with PS hemispheres (after heat treatment), and glass with PS/ZnO hierarchical structure, respectively, under the illumination of 473 nm laser at the same incident angle of 60° (larger than the critical angle θ_c = 43.0°). The blank silica glass substrate demonstrated obvious TIR, as shown in Figure 6a. In Figure 6b and c, one can find that a small fraction of the light transmitted to air from the glass substrates covered with PS microspheres or PS hemispheres. Most of the light was still totally reflected at the inner surface of the glass substrates. In Figure 6d, it is illustrated that a significant amount of light otherwise trapped

DOI: 10.1021/acsami.5b04911
ACS Appl. Mater. Interfaces 2015, 7, 19179–19188

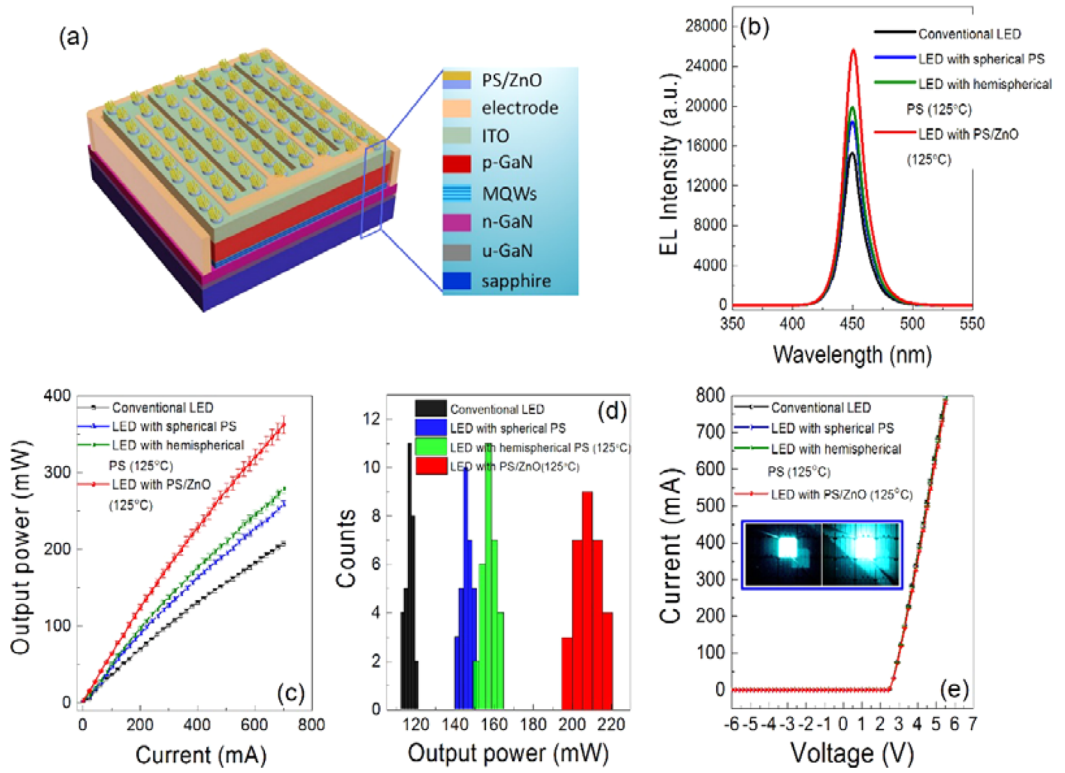

Figure 7. (a) Three-dimensional schematic of a single LED chip produced using the conventional LED fabrication technique. (b) EL spectra of conventional LED, LED with PS microspheres, LED with PS hemispheres, and LED with PS/ZnO hierarchical structure. (c) LOP versus forward current curves. (d) Histograms of light-output power (LOP) measured from a set of four kinds of LEDs, with each kind of LED composed of 30 separate chips. (e) Measured $I-V$ curves of LEDs. The insets show emission images of conventional LED and LED with PS/ZnO hierarchical structure at an injection current of 10 mA.

due to TIR could be extracted out and transmitted to the air. The light-extraction ability was much enhanced as compared with those covered with PS microspheres, although there was still some fraction of TIR occurred.

To quantitatively measure the incident angular-dependent light-transmission behaviors of the fabricated structures, an integrating sphere was located close to the glass substrates to collect the total extracted light through the PS/ZnO hierarchical structures. In Figure 6e, the transmission efficiency was shown as a function of incident angle of the laser light, with a comparison with those of the blank silica glass substrate and the glass covered with PS microparticles (spheres or hemispheres). Obviously, significant transmission efficiency was obtained in the large incident angle range beyond the critical angle when the glass substrate was covered either with PS microparticles or with PS/ZnO hierarchical structures. Generally, microparticles can directly serve as microlens arrays for enhancing light extractions, because they provide enlarged effective photon escape cones due to their convex lens shapes.[16,40,41] Furthermore, the refractive index of PS is 1.59 in the visible spectrum. A submonolayer of PS microparticles on silica glass surface can thus act as a graded refractive index antireflection coating matching the refractive index between glass and air. Therefore, for the PS microparticle layers coating on silica glass surface, the enhanced light extraction beyond the critical angle should be attributed to the effects of reduced Fresnel reflection as well as the enlarged effective photon escape cone induced by them.[7] It can be found that the light transmission is slightly higher for the PS hemisphere coatings than that for the PS microsphere coating. This can be attributed to the effect of heat treatment, which induces changes on the effective refractive index as well as the contact way of the PS microspheres to the substrate. For the PS microsphere monolayer, heat treatment results in larger effective refractive index due to the gradually changed area fractions of air and PS microspheres at a certain height.[38] For the silica glass prism covered with PS/ZnO hierarchical structures, light transmittance was much greater than that of the PS microparticle-covered samples when the light incident angle was beyond the critical angle. This result could be attributed to the cooperative effect of the PS hemisphere arrays that act as microlens and the ZnO nanoparticle porous layers that generate enhanced Rayleigh scattering. The refractive index of ZnO is as high as 2.11.[42] Previous research showed that there was significant enhanced light scattering in the nanoporous structures with columnar aggregation of nanoparticles of high refractive index materials, due to the coherent Rayleigh scattering from the particles that were very closely piled and the strong contrast in the refractive index between the nanopores and the nanoparticles.[30] The enhanced scattering effect of the nanoscale structures could work with the microlens effect of the microscale structures concurrently and cooperatively. As a result, a dual enhancement of LEE was realized.

3.4. Applied for Light Extraction of GaN-Based LEDs.

The excellent light-extraction properties of the PS/ZnO hierarchical structures were applied for improving the LEE of GaN-based LEDs. The structure of the GaN-based LED device used in this study is shown in Figure 7a schematically. PS microsphere layers as well as PS/ZnO micronano hierarchical structure were fabricated on the top of the LED chips. The

DOI: 10.1021/acsami.5b04911
ACS Appl. Mater. Interfaces 2015, 7, 19179−19188

Table 1. Light-Output Power (LOP) and Forward Voltage of the Four Types of LEDs at Injection Currents of 350 and 700 mA

	LOP (mW)/ 350 mA	enhancement/ 350 mA	forward voltage (V)/ 350 mA	LOP (mW)/ 700 mA	enhancement/ 700 mA	forward voltage (V)/ 700 mA
conventional LED	116.8 ± 2.0		3.928 ± 0.029	207.1 ± 3.6		5.145 ± 0.038
LED with spherical PS	145.5 ± 2.7	24.6% ± 4.4%	3.949 ± 0.032	258.5 ± 4.8	24.8% ± 4.4%	5.168 ± 0.044
LED with hemispherical PS	157.2 ± 3.5	34.6% ± 5.4%	3.949 ± 0.032	279.1 ± 6.2	34.8% ± 5.4%	5.168 ± 0.045
LED with PS/ZnO	207.6 ± 6.3	77.7% ± 8.5%	4.000 ± 0.038	362.7 ± 11.0	75.1% ± 8.5%	5.221 ± 0.049

optical properties and electric properties of the LEDs were measured for comparison. Figure 7b shows the electroluminescence (EL) spectra of the LED chips, which include the original LED chip, and the LED chips covered with PS microspheres or hemispheres, as well as the LED chip covered with PS/ZnO hierarchical structure, at an injection current of 350 mA. Each curve shows the average result over the measurements on 30 LED chips. The four curves have similar EL bands; there is neither significant shift on the peak wavelength (at ∼450 nm) nor broadening of the peak width (with a full width at half-maximum (fwhm) of ∼20 nm). Compared to the original LED chips, the LED chips with PS microspheres or PS hemispheres both have an enhanced EL intensity. Nevertheless, the EL intensity of the LED chip with PS/ZnO hierarchical structure exhibit a much larger extra enhancement on the basics of the enhanced EL of LED covered with PS microspheres or hemispheres.

Figure 7c shows the typical LOP versus forward current curves of the four kinds of LED chips. The error bars shown in the figure were determined from a statistical analysis of the data measured from 30 separate LED chip cells. Figure 7d includes histograms showing the distribution of light-output power measured from a set of four kinds of LEDs, with each kind of LED composed of 30 separate chips. We can see that the histograms of each kind of chip all resemble a normal distribution with standard deviations of 2.0, 2.7, 3.5, and 6.3 mW, respectively. Although the standard deviations of the LOP data measured from the chips fabricated with PS microspheres or PS/ZnO hierarchical structures become significantly increased, due to the local fluctuation of the fabricating conditions, no significant overlaps among the distributions of the light-output power for the four different types of chips could be observed. It therefore indicates that a real improvement on the LOP is realized for the LED chips covered with PS microspheres, as well as for the LED chips covered with PS/ZnO hierarchical structures.[43]

Figure 7e shows the current−voltage (I−V) curves of the four kinds of LED chips measured at room temperature. The error bars of the data were determined with a similar procedure as that used for the statistical analysis of LOP data. We can see that all the I−V curves are almost overlapped. These results indicate that the deposition of PS microstructure or PS/ZnO micronano hierarchical structure does not significantly degrade the electrical properties of the GaN-based LEDs.

In Table 1, the data of LOP and forward voltage for the four types of LEDs measured at forward currents of 350 and 700 mA are compared. At 350 mA forward current, the LOPs of the conventional LED, LED with PS microspheres, LED with PS hemispheres, and LED with PS/ZnO hierarchical structure are 116.8 ± 2.0, 145.5 ± 2.7, 157.2 ± 3.5, and 207.6 ± 6.3 mW, respectively. The latter three each have a 24.6%, 34.6%, and 77.7% LOP enhancement, respectively. Clearly, with PS/ZnO hierarchical structure, very high light-output power improvement was realized. The physical mechanisms of such a large enhancement could be attributed to the synergistic effect in the hierarchical surface feature combining microscale and nanoscale structures. As we have analyzed above, the PS microparticle arrays could act as microlens, which have been proven as an effective way to reduce internal light reflection, and the effect could be modeled with ray tracing.[44,45] With a layer of PS microparticles on ITO surface of LED, the light-output power of the LED could be significantly increased due to the increase in its effective photon escape cone. Furthermore, a submonolayer coating of PS microspheres could also reduce Fresnel reflection on the ITO/air interface, due to the formation of graded refractive index profile, which transits from ITO (n = 2.2) to air (n = 1). LED covered with PS hemisphere layers could have a more increased output power than the LED covered with PS microspheres, due to the increased effective refractive index result from the enhanced contact area of the PS hemispheres.[38]

On the other hand, for the porous ZnO nanoparticle layer, we have to consider another light-extracting mechanism. Because the effective refractive index of the ZnO nanoparticle layers is much larger than that of air, light which otherwise totally internally reflected in the ITO substrate can significantly escape and enter the ZnO nanoparticle layer. Light scattering (Rayleigh scattering) induced by strong refractive index contrast among the random distribution of ZnO nanoparticle columns and nanometer-sized pores is therefore responsible for the light-output enhancement. Such a mechanism has been demonstrated in our previous studies.[30] Furthermore, the columnar piling of ZnO nanoparticles in the porous layer induces excess optical scatterings, due to the coherent scatterings from the nanoparticles that are very closely piled. Such coherent scatterings result in effective cross sections that are larger than the sum of the Rayleigh scattering cross section of the individual nanoparticles.

Incorporating ZnO nanoparticle porous layers with the PS microstructures generates much greater LOP enhancement, which should be attributed to the cooperative effect between the PS microlens and the ZnO nanoparticle scatters. Because the TIR-depressing mechanisms of microscale and nanoscale structures are basically different, light-extraction enhancement with porous ZnO nanoparticle coating could function with the photon escape cone enlarging effect of the PS microsphere layers on parallel to generate an additional enhancement. Therefore, a dual enhancement of LOP was achieved.

Recently, various nanostructures have been investigated for improving the LOP of LEDs. Kim et al. reported an improvement of light-extraction efficiency from GaN-based LEDs using a hybrid structure composed of ZnO nanorod arrays and NiCoO nanoparticle arrays grown on the p-GaN layer.[29] Lin et al. observed a 26.4% LOP enhancement from the LED covered with ITO nanorod arrays fabricated by oblique-angle deposition technique.[32] However, in these studies, the light-extraction effects of the nanostructures, such as the waveguiding effect, multiple tilted surfaces, and the graded

DOI: 10.1021/acsami.5b04911
ACS Appl. Mater. Interfaces 2015, 7, 19179−19188

refractive indices, were considered independently. The structures were not optimized to apply the cooperative effect between the microscale structures and the nanoscale structure. Although light scattering was sometime considered, the fabricated structures were also not optimized for scattering enhancement. Our present strategy provided an effective way for improving the LOP of LEDs by incorporating the microscale and nanoscale light-extraction mechanisms. Furthermore, we demonstrated that porous piling of nanoparticles with high refractive index could be powerful Rayleigh scatters for light extraction.

Figure 8 shows the far-field radiation profiles of the four types of LEDs. The direction perpendicular to the surface of the LED is defined as zero degree. Compared with that of the conventional LEDs, the light-output intensities of LEDs with PS microparticles (spheres and hemispheres) show obvious enhancement in the angular range from 0° to 50°, and the greatest light intensity is in the vertical direction. Such enhancement behavior can be attributed to the microlens effect and the formation of a graded refractive index profile of the PS microstructures. According to Snell's law, the critical angle for light output from ITO (n = 2.2 at 450 nm) to air is only 27°. When PS microparticle arrays are fabricated on the ITO surface of an LED, the critical angle is 46.3° for light output from ITO to PS microlens (n = 1.59 at 450 nm) and 40° for light output from PS microlens to the air, respectively. Thus, the photon escape cone of the LEDs could be enlarged. In addition, a PS microparticle layer on the LED surface can provide graded refractive index transition from ITO to air, and Fresnel reflection will be reduced in the vertical direction. For an LED with PS/ZnO hierarchical structure, the light-output intensity distribution shows an obvious enhancement in the angular range from 0° to 70° compared with the conventional LED, which indicates that fabricating PS/ZnO hierarchical structure on the surface of LED could further enlarge the photon escape cone. The enhancement is relatively homogeneous at the whole angular range. In addition, the enhancement can be extended to the angular range, which is obviously greater than that of LED with PS microspheres/hemispheres only. This behavior can be attributed to the enhanced Rayleigh scattering effect of the ZnO porous nanoparticle layers. It therefore demonstrates another effective approach for the enhancement of light extraction, that is, an increase in the radiation profile width. This Lambertian light emission is beneficial to the applications in general lighting.[28]

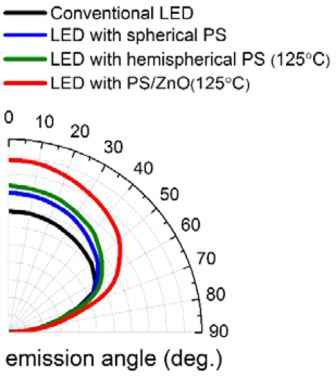

Figure 8. Far-field radiation profiles of the four types of LEDs.

4. CONCLUSION

In summary, we have fabricated PS/ZnO micronano hierarchical structures on the surface of GaN-based LEDs to enhance the light-extraction efficiency (LEE). The hierarchical structure was composed of randomly distributed submicron-sized spherical/hemipherical PS particles and porous accumulations of nanometer-sized ZnO particles, which were fabricated by performing gas-phase cluster beam deposition at glancing incidence. Incident angle-resolved light-transmission measurements showed that light transmission from the internal of the medium could be tremendously enhanced for light incident beyond the critical angle of total internal reflection at the medium−air interface with the covering of the PS/ZnO hierarchical structures. The light-transmission enhancement could be attributed to the cooperative mechanism that combines the microlens function of the PS microspheres and the enhanced Rayleigh scattering provided by the columnar aggregation of the ZnO nanoparticles. The LOP of the GaN-based LED with PS/ZnO hierarchical structure has been improved by 77.7% as compared with the unmodified LED. The LOP enhancement comes from the fact that the PS/ZnO micronano hierarchical structures can effectively attract the emitting light that was otherwise trapped in the LED due to total internal reflection. Our research demonstrates a scalable, cost-effective fabrication technique that might provide a viable solution for achieving better light extraction in the existing solid-state lighting devices.

AUTHOR INFORMATION

Corresponding Author

*sjhanmin@nju.edu.cn.

Notes

The authors declare no competing financial interest.

ACKNOWLEDGMENTS

The authors thank the National Natural Science Foundation of China (Grant no. 51171077), the National Basic Research Program of China (973 Program, Grant no. 2014CB932302), and the Scientific Research Foundation of Graduated School of Nanjing University (Grant no. 2013CL10). This research was also supported by the Jiangsu Province Innovation Fund for Technology Based Firms (BC2013118) and a project funded by the Priority Academic Program Development of Jiangsu Higher Education Institutions.

REFERENCES

(1) Hyun, W. J.; Lee, H. K.; Oh, S. S.; Hess, O.; Choi, C.-G.; Im, S. H.; Park, O. O. Two-Dimensional TiO_2 Inverse Opal with a Closed Top Surface Structure for Enhanced Light Extraction from Polymer Light-Emitting Diodes. *Adv. Mater.* **2011**, *23* (16), 1846−1850.

(2) Wiesmann, C.; Bergenek, K.; Linder, N.; Schwarz, U. T. Photonic Crystal LEDs-Designing Light Extraction. *Laser Photonics Rev.* **2009**, *3* (3), 262−286.

(3) Okamoto, K.; Niki, I.; Shvartser, A.; Narukawa, Y.; Mukai, T.; Scherer, A. Surface-Plasmon-Enhanced Light Emitters Based on InGaN Quantum Wells. *Nat. Mater.* **2004**, *3* (9), 601−605.

(4) Nishida, T.; Saito, H.; Kobayashi, N. Efficient and High-Power AlGaN-Based Ultraviolet Light-Emitting Diode Grown on Bulk GaN. *Appl. Phys. Lett.* **2001**, *79* (6), 711−712.

(5) Zhao, H.; Liu, G.; Zhang, J.; Poplawsky, J. D.; Dierolf, V.; Tansu, N. Approaches for High Internal Quantum Efficiency Green InGaN Light-Emitting Diodes with Large Overlap Quantum Wells. *Opt. Express* **2011**, *19* (14), A991−A1007.

DOI: 10.1021/acsami.5b04911
ACS Appl. Mater. Interfaces 2015, 7, 19179−19188

(6) Hsiao, Y.-H.; Chen, C.-Y.; Huang, L.-C.; Lin, G.-J.; Lien, D.-H.; Huang, J.-J.; He, J.-H. Light Extraction Enhancement with Radiation Pattern Shaping of LEDs By Waveguiding Nanorods with Impedance-Matching Tips. *Nanoscale* **2014**, *6* (5), 2624−2628.
(7) Geng, C.; Wei, T.; Wang, X.; Shen, D.; Hao, Z.; Yan, Q. Enhancement of Light Output Power from LEDs Based on Monolayer Colloidal Crystal. *Small* **2014**, *10* (9), 1668−1686.
(8) Do, Y. R.; Kim, Y. C.; Song, Y. W.; Cho, C. O.; Jeon, H.; Lee, Y. J.; Kim, S. H.; Lee, Y. H. Enhanced Light Extraction From Organic Light-Emitting Diodes with 2D SiO_2/SiN_x Photonic Crystals. *Adv. Mater.* **2003**, *15* (14), 1214−1218.
(9) Wierer, J. J., Jr.; David, A.; Megens, M. M. III-Nitride Photonic-Crystal Light-Emitting Diodes with High Extraction Efficiency. *Nat. Photonics* **2009**, *3* (3), 163−169.
(10) Fu, P.-H.; Lin, G.-J.; Wang, H.-P.; Lai, K.-Y.; He, J.-H. Enhanced Light Extraction of Light-Emitting Diodes via Nano-Honeycomb Photonic Crystals. *Nano Energy* **2014**, *8*, 78−83.
(11) Zhu, Z.; Wu, S.; Xue, C.; Zhao, J.; Wang, L.; Wu, Y.; Liu, B.; Cheng, C.; Gu, M.; Chen, H.; Tai, R. Enhanced Light Extraction of Scintillator Using Large-Area Photonic Crystal Structures Fabricated by Soft-X-Ray Interference Lithography. *Appl. Phys. Lett.* **2015**, *106* (24), 241901.
(12) Sheu, J. K.; Hung, I. H.; Lai, W. C.; Shei, S. C.; Lee, M. L. Enhancement in Output Power of Blue Gallium Gitride-Based Light-Emitting Diodes with Omnidirectional Metal Reflector Under Electrode Pads. *Appl. Phys. Lett.* **2008**, *93* (10), 103507.
(13) Lee, K. H.; Moon, Y.-T.; Song, J.-O.; Kwak, J. S. Light Interaction in Sapphire/MgF_2/Al Triple-Layer Omnidirectional Reflectors in AlGaN-Based Near Ultraviolet Light-Emitting Diodes. *Sci. Rep.* **2015**, *5*, 9717.
(14) Ee, Y.-K.; Arif, R. A.; Tansu, N.; Kumnorkaew, P.; Gilchrist, J. F. Enhancement of Light Extraction Efficiency of InGaN Quantum Wells Light Emitting Diodes Using SiO_2/Polystyrene Microlens Arrays. *Appl. Phys. Lett.* **2007**, *91* (22), 221107.
(15) Yang, J. P.; Bao, Q. Y.; Xu, Z. Q.; Li, Y. Q.; Tang, J. X.; Shen, S. Light Out-Coupling Enhancement of Organic Light-Emitting Devices with Microlens Array. *Appl. Phys. Lett.* **2010**, *97* (22), 223303.
(16) Ee, Y.-K.; Kumnorkaew, P.; Arif, R. A.; Tong, H.; Zhao, H.; Gilchrist, J. F.; Tansu, N. Optimization of Light Extraction Efficiency of III-Nitride LEDs With Self-Assembled Colloidal-Based Microlenses. *IEEE J. Sel. Top. Quantum Electron.* **2009**, *15* (4), 1218−1225.
(17) Chuang, S.-H.; Tsung, C.-S.; Chen, C.-H.; Ou, S.-L.; Horng, R.-H.; Lin, C.-Y.; Wuu, D.-S. Transparent Conductive Oxide Films Embedded with Plasmonic Nanostructure for Light-Emitting Diode Applications. *ACS Appl. Mater. Interfaces* **2015**, *7* (4), 2546−2553.
(18) Homeyer, E.; Mattila, P.; Oksanen, J.; Sadi, T.; Nykanen, H.; Suihkonen, S.; Symonds, C.; Tulkki, J.; Tuomisto, F.; Sopanen, M.; Bellessa, J. Enhanced Light Extraction from InGaN/GaN Quantum Wells with Silver Gratings. *Appl. Phys. Lett.* **2013**, *102* (8), 081110.
(19) Chiu, N.-F.; Yang, C.-D.; Kao, Y.-L.; Lu, K.-L. Enhancing Extraction of Light from Metal Composite Structures for Plasmonic Emitters Using Light-Coupling Effect. *Opt. Express* **2015**, *23* (8), 9602−9611.
(20) Huang, J.-K.; Liu, C.-Y.; Chen, T.-P.; Huang, H.-W.; Lai, F.-I.; Lee, P.-T.; Lin, C.-H.; Chang, C.-Y.; Kao, T. S.; Kuo, H.-C. Enhanced Light Extraction Efficiency of GaN-Based Hybrid Nanorods Light-Emitting Diodes. *IEEE J. Sel. Top. Quantum Electron.* **2015**, *21* (4), 6000107.
(21) Lin, N.-M.; Shei, S.-C.; Chang, S.-J. Solution-Growth ZnO Nanorods for Light Extraction in GaN-Based Flip-Chip LEDs. *ECS Solid State Lett.* **2015**, *4* (4), R23−R25.
(22) Horng, R. H.; Yang, C. C.; Wu, J. Y.; Huang, S. H.; Lee, C. E.; Wuu, D. S. GaN-Based Light-Emitting Diodes with Indium Tin Oxide Texturing Window Layers Using Natural Lithography. *Appl. Phys. Lett.* **2005**, *86* (22), 221101.
(23) Park, H.-H.; Zhang, X.; Cho, Y.; Kim, D.-W.; Kim, J.; Lee, K. W.; Choi, J.; Lee, H. K.; Jung, S. H.; Her, E. J.; Kim, C. H.; Moon, A. Y.; Shin, C.-S.; Shin, H.-B.; Sung, H. K.; Park, K. H.; Park, H.-H.; Kim, H.-J.; Kang, H. K. Wafer-Scale Surface Roughening for Enhanced Light Extraction of High Power AlGaInP-Based Light-Emitting Diodes. *Opt. Express* **2014**, *22* (9), A723−A734.
(24) Wang, P.; Cao, B.; Wei, W.; Gan, Z.; Liu, S. Improved Light Extraction of GaN-Based Light-Emitting Diodes by ITO Patterning with Optimization Design. *Solid-State Electron.* **2010**, *54* (3), 283−287.
(25) Leung, S.-F.; Zhang, Q.; Xiu, F.; Yu, D.; Ho, J. C.; Li, D.; Fan, Z. Light Management with Nanostructures for Optoelectronic Devices. *J. Phys. Chem. Lett.* **2014**, *5* (8), 1479−1495.
(26) Sheu, J.-K.; Lu, Y. S.; Lee, M.-L.; Lai, W. C.; Kuo, C. H.; Tun, C.-J. Enhanced Efficiency of GaN-Based Light-Emitting Diodes with Periodic Textured Ga-Doped ZnO Transparent Contact Layer. *Appl. Phys. Lett.* **2007**, *90* (26), 263511.
(27) Lee, Y.-C.; Kuo, H.-C.; Cheng, B.-S.; Lee, C.-E.; Chiu, C.-H.; Lu, T.-C.; Wang, S.-C.; Liao, T.-F.; Chang, C.-S. Enhanced Light Extraction in Wafer-Bonded AlGaInP-Based Light-Emitting Diodes via Micro- and Nanoscale Surface Textured. *IEEE Electron Device Lett.* **2009**, *30* (10), 1054−1056.
(28) Ho, C.-H.; Hsiao, Y.-H.; Lien, D.-H.; Tsai, M. S.; Chang, D.; Lai, K.-Y.; Sun, C.-C.; He, J.-H. Enhanced Light-Extraction from Hierarchical Surfaces Consisting of p-GaN Microdomes and SiO_2 Nanorods for GaN-Based Light-Emitting Diodes. *Appl. Phys. Lett.* **2013**, *103* (16), 161104.
(29) Kim, D.-H.; Shin, D. S.; Park, J. Enhanced Light Extraction from GaN Based Light-Emitting Diodes Using a Hemispherical NiCoO Lens. *Opt. Express* **2014**, *22* (13), A1071−A1078.
(30) Mao, P.; Sun, F.; Yao, H.; Chen, J.; Zhao, B.; Xie, B.; Han, M.; Wang, G. Extraction of Light Trapped Due to Total Internal Reflection Using Porous High Refractive Index Nanoparticle Films. *Nanoscale* **2014**, *6* (14), 8177−8184.
(31) Mao, P.; Xu, M.; Chen, J.; Xie, B.; Song, F.; Han, M.; Wang, G. Dual Enhancement of Light Extraction Efficiency of Flip-Chip Light-Emitting Diodes with Multiple Beveled SiC Surface and Porous ZnO Nanoparticle Layer Coating. *Nanotechnology* **2015**, *26* (18), 185201.
(32) Lin, C.-C.; Lee, C.-T. Enhanced Light Extraction of GaN-Based Light Emitting Diodes Using Nanorod Arrays. *Electrochem. Solid-State Lett.* **2010**, *13* (8), H278−H280.
(33) Yin, Z.; Liu, X.; Yao, H.; Wu, Y.; Hao, X.; Han, M.; Xu, X. Light Extraction Enhancement of GaN LEDs by Hybrid ZnO Micro-Cylinders and Nanorods Array. *IEEE Photonics Technol. Lett.* **2013**, *25* (20), 1989−1992.
(34) Mao, P.; Chen, J.; Zhou, Y.; Liao, K.; Zhao, B.; Han, J.; Wang, G.; Han, M. Anisotropy Antireflection TiO_2 Nanoparticle Films Fabricated with Directed Cluster Beam Deposition. *Phys. Status Solidi C* **2012**, *9* (12), 2366−2369.
(35) Han, M.; Xu, C.; Zhu, D.; Yang, L.; Zhang, J.; Chen, Y.; Ding, K.; Song, F.; Wang, G. Controllable Synthesis of Two-Dimensional Metal Nanoparticle Arrays with Oriented Size and Number Density Gradients. *Adv. Mater.* **2007**, *19* (19), 2979−2983.
(36) Haberland, H.; Mall, M.; Moseler, M.; Qiang, Y.; Reiners, T.; Thurner, Y. Filling of Micron-Sized Contact Holes with Copper by Energetic Cluster-Impact. *J. Vac. Sci. Technol., A* **1994**, *12* (5), 2925−2930.
(37) Fu, X.-X.; Kang, X.-N.; Zhang, B.; Xiong, C.; Jiang, X.-Z.; Xu, D.-S.; Du, W.-M.; Zhang, G.-Y. Light Transmission from the Large-Area Highly Ordered Epoxy Conical Pillar Arrays and Application to GaN-Based Light Emitting Diodes. *J. Mater. Chem.* **2011**, *21* (26), 9576−9581.
(38) Choi, H. K.; Yang, Y. J.; Park, O. O. Hemispherical Arrays of Colloidal Crystals Fabricated by Transfer Printing. *Langmuir* **2014**, *30* (1), 103−109.
(39) Zhou, L.; Ou, Q.-D.; Chen, J.-D.; Shen, S.; Tang, J.-X.; Li, Y.-Q.; Lee, S.-T. Light Manipulation for Organic Optoelectronics Using Bio-inspired Moth's Eye Nanostructures. *Sci. Rep.* **2014**, *4*, 4040.
(40) Wrzesniewski, E.; Eom, S.-H.; Cao, W.; Hammond, W. T.; Lee, S.; Douglas, E. P.; Xue, J. Enhancing Light Extraction in Top-Emitting Organic Light-Emitting Devices Using Molded Transparent Polymer Microlens Arrays. *Small* **2012**, *8* (17), 2647−2651.
(41) Lee, H. K.; Ko, Y. H.; Raju, G. S. R.; Yu, J. S. Light-Extraction Enhancement and Directional Emission Control of GaN-Based LEDs

DOI: 10.1021/acsami.5b04911
ACS Appl. Mater. Interfaces 2015, 7, 19179−19188

by Self-Assembled Monolayer of Silica Spheres. *Opt. Express* **2012**, *20* (22), 25058−25063.
(42) Jeong, H.; Park, D. J.; Lee, H. S.; Ko, Y. H.; Yu, J. S.; Choi, S.-B.; Lee, D.-S.; Suh, E.-K.; Jeong, M. S. Light-Extraction Enhancement of a GaN-Based LED Covered with ZnO Nanorod Arrays. *Nanoscale* **2014**, *6* (8), 4371−4378.
(43) Luber, E. J.; Buriak, J. M. Reporting Performance in Organic Photovoltaic Devices. *ACS Nano* **2013**, *7* (6), 4708−4714.
(44) Lee, S. J. Analysis of Light-Emitting Diodes by Monte Carlo Photon Simulation. *Appl. Opt.* **2001**, *40* (9), 1427−1437.
(45) Zhmakin, A. I. Enhancement of Light Extraction from Light Emitting Diodes. *Phys. Rep.* **2011**, *498* (4−5), 189−241.

DOI: 10.1021/acsami.5b04911
ACS Appl. Mater. Interfaces 2015, 7, 19179−19188